

Coaxial electrospun PGS/PCL and PGS/PGS-PCL nanofibrous membrane containing platelet-rich plasma for skin tissue engineering

Shima Shafizadeh, Parisa Heydari, Anousheh Zargar Kharazi & Laleh Shariati

To cite this article: Shima Shafizadeh, Parisa Heydari, Anousheh Zargar Kharazi & Laleh Shariati (08 Jan 2024): Coaxial electrospun PGS/PCL and PGS/PGS-PCL nanofibrous membrane containing platelet-rich plasma for skin tissue engineering, Journal of Biomaterials Science, Polymer Edition, DOI: [10.1080/09205063.2023.2299073](https://doi.org/10.1080/09205063.2023.2299073)

To link to this article: <https://doi.org/10.1080/09205063.2023.2299073>



Published online: 08 Jan 2024.



Submit your article to this journal [↗](#)



Article views: 3




View related articles [↗](#)



View Crossmark data [↗](#)



Coaxial electrospun PGS/PCL and PGS/PGS-PCL nanofibrous membrane containing platelet-rich plasma for skin tissue engineering

Shima Shafizadeh^a, Parisa Heydari^b, Anousheh Zargar Kharazi^{a,b}  and Laleh Shariati^{a,c}

^aBiomaterials Nanotechnology and Tissue Engineering Faculty, School of Advanced Technologies in Medicine, Isfahan University of Medical Sciences, Isfahan, Iran; ^bApplied Physiology Research Center, Isfahan University of Medical Sciences, Isfahan, Iran; ^cBiosensor Research Center, Isfahan University of Medical Sciences, Isfahan, Iran

ABSTRACT

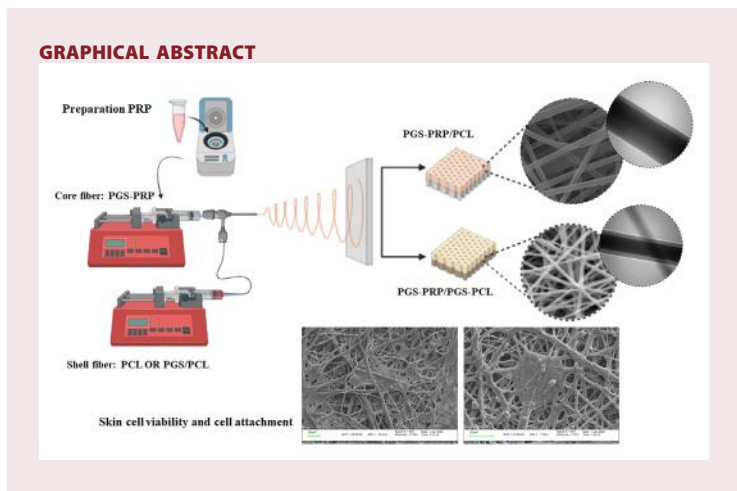
Wound healing will be enhanced using structures with therapeutic effects. This study fabricated a novel nanofibrous scaffold for skin tissue regeneration using a coaxial structure polyglycerol sebacate (PGS)/platelet-rich plasma (PRP) was embedded in the core and two different compositions were selected for the shell; in one group, polycaprolactone (PCL), and in the other group, PGS/PCL blend was used. The physical, mechanical behavior, drug delivery patterns, and cell response of scaffolds were evaluated. Results revealed that by adding PRP to the core and PGS to the shell, fiber diameters decreased to 260.8 ± 31.3 nm. It also decreased the water contact angle from 66° to 32° , that is ideal candidate for cell attachment. The drug release showed a burst release pattern in the first 30 min, followed by a continuous and slow release during the first day. Adding PGS to the shell decreased the elastic modulus, and its value reached about 500 kPa, which is near the skin elastic modulus and will lead to greater mechanical compatibility for cell proliferation. Particularly, the addition of PRP to the fiber structure enhanced the cell viability and cell adhesion with a suitable morphology. Based on the results, nanofibrous PGS-PRP/PGS-PCL dressing can enhance skin tissue regeneration.

ARTICLE HISTORY

Received 13 September 2023
Revised 18 December 2023
Accepted 20 December 2023

KEYWORDS

Skin tissue engineering; pRP; coaxial electrospinning; pGS; pCL



1. Introduction

The skin tissue provides a physiological barrier against temperature alterations, mechanical stresses, and various physiological functions to protect internal organs [1]. Healthy skin can damage through chemical and biological agents and induce skin defects such as inflammation, chronic wounds, and allergies [2]. A superior wound dressing or biological agents are needed to accelerate the wound healing process [3]. As a result, it is imperative that novel dressings with bioactive ingredients be developed in order to speed up wound healing [4]. One ideal candidate for wound dressing is the highly porous nanofibers structure with enhanced water absorption and mechanical and biocompatible properties [5,6]. The coaxial electrospinning process is an efficient technique for producing micro-nanofibers in various wound dressings with a high surface-to-volume ratio. In this method, it is possible to loading polymers, drugs, proteins, and biological agents that cannot be electrospinning [7,8]. The core-shell electrospinning process employs an inner needle for the core and an outer needle for the shell, with two separate solutions able to creating one fiber at the same time [9], as Su et al. [10] investigated the core-shell fibers of poly caprolactone/polyethylene oxide as shell and keratin/hyaluronic acid as the core of fibers. They demonstrated that the hydrophilic polymer could not be electrospinning easily, formed in coaxial fibers structure, and be suitable for wound healing application.

In recent years, Poly (glycerol sebacate) (PGS) has been the focus of many studies as a biodegradable and elastomeric polymer because of its biocompatibility and linear hydrolysis degradation profile [11]. PGS has similar mechanical properties to elastin and collagen, making it suitable for regenerating soft tissues [12,13]. Frydrych et al. [14] studied the physical and mechanical behavior of PGS/poly lactic acid (PLA) scaffolds for soft tissue regeneration application. Their results demonstrated that these combinations of polymers have ideal hydrophilic, appropriate mechanical properties and increased cell penetration for soft tissue engineering.

A wide range of synthesis polymers have been used for electrospinning due to biodegradability, biocompatibility, and suitable formation[15]. Among the synthesis polymers, poly caprolactone (PCL) is an ideal choice for fabricating skin tissue engineering

scaffolds through electrospinning because of its mechanical properties, biocompatibility, and controllable biodegradability [16–18]. Ehterami et al. [19] evaluated electrospun Collagen/Chitosan/PCL nanoparticle samples for wound healing application. They demonstrated that the PCL with electrospinning ability blended with Collagen and chitosan provides ideal vapor permeability, wettability, mechanical properties, cellular behavior, and blood compatibility for full-thickness and chronic wound treatment.

In addition to suitable properties of polymers, drugs or biological agents are necessary to accelerate wound healing [20]. Recently, platelet-rich plasma (PRP) has been an ideal candidate for wound healing applications and promoting the healing of various defects [21]. PRP is interesting for wound healing and tissue engineering, due to the high concentration of various substances and growth factors such as transforming growth factor (TGF-1), platelet-derived growth factor (PDGF), epidermal growth factor (EGF), vascular endothelial growth factor (VEGF), insulin-like growth factor (IGF), and basic fibroblast growth factor (bFGF) [22]. Zhang et al. [23] demonstrated that dual-network hydrogel with PRP could promote wound healing through re-epithelialization, increasing growth factor levels, and early transition of wound healing, control inflammation response, and angiogenesis stages. Similarly, Shi et al. [24] fabricated a wound dressing of carboxyl methyl cellulose (CMC), gentamycin sulfate, and PRP for infected wounds treatment. Its results demonstrated that this wound dressing could reduce bacterial infection, inhibit pro-inflammatory factors like IL-6 and TNF- α , and enhance anti-inflammatory factors like TGF- β . These findings showed that PRP has great potential in managing chronic wounds. Accordingly, in this study, we fabricated wound dressing based on PGS/PCL and PGS/PGS-PCL coaxial fibers containing PRP in the core of fibers. In this regard, after the synthesis of PGS, and extraction PRP of human blood, the coaxial electrospinning PGS/PCL and PGS/PGS-PCL with or without PRP were applied to fabricate ideal scaffolds for skin tissue regeneration. Additionally, polymers and PRP were investigated for their chemical, mechanical, physical, and biological properties when used in wound dressings.

2. Materials and methods

2.1. Materials

In this study, Sebacic acid (99%, Merck, Germany), Glycerol (99%, Merck, Germany), poly (3-caprolactone) (PCL) (Sigma-Aldrich), chloroform (Sigma-Aldrich), Acetone (Merck, Germany), Dimethyl thiazole diphenyltetrazolium bromide (MTT, Sigma-Aldrich), sodium citrate (Vacuette, Switzerland), dimethyl sulfoxide (DMSO) (Merck, Germany), fetal bovine serum (FBS), Dulbecco's Modified Eagle Medium (DMEM-high), penicillin, streptomycin (Bioidea, Iran), and phosphate buffered saline tablets (PBS, Sigma-Aldrich) were purchased.

2.2. Synthesis poly glycerol sebacate (PGS)

Polyglycerol sebacate (PGS) has been synthesized, according to previous studies[25]. In simple terms, sebacic acid and glycerol monomers were used to condensate polymerize the PGS polymer. Sebacic acid and glycerol were combined in a 1:1 molar ratio, and

the mixture was heated at 120°C for 24h *via* an N₂ environment while the reactant was maintained at 40°C. A white-colored, viscous PGS polymer ultimately resulted [7].

2.3. Platelet-rich plasma (PRP) preparation

Peripheral blood samples were collected from healthy volunteers in 9 ml tubes containing 3.8% sodium citrate. Extraction and optimization of PRP were done by centrifuge in two steps. Following the first spin at 200g for 10 min, the liquid supernatant was transferred to another tube and the second spin was done at 2500g for 15 min. As a result, the upper two-thirds of the supernatant is removed, and the platelet pellets are suspended in the lower third of the plasma. It's PRP [26].

2.4. Preparation of electrospun PGS-PRP/PCL and PGS-PRP/PGS-PCL core-shell fibers

To prepare the PGS/PCL scaffolds, PCL and PGS were dissolved separately in chloroform (CF) and acetone solvents (volume ratio of 8:2) at a concentration of 20% wt and 10% wt, respectively. Afterwards, the PGS and PCL solutions were mixed for 30 min at 37°C on a magnetic stirrer, separately. The PRP was added to the core (PGS solution) with 0.5% w/v and was mixed for 10 min. The core and shell flow rates, voltage and tip to collector distance were 0.15 mL/h, 2 mL/h, 12 kV, and 18 cm, respectively. To fabricate the core-shell samples, the PGS or PGS/PRP solution and PCL solution were electrospun on a coaxial needle (G16 outer diameter (OD) = 1.20 mm and G23 inner diameter (ID) = 0.33 mm).

On the other site, to fabricate the PGS/PGS-PCL and PGS-PRP/PGS-PCL samples, the PCL and PGS with 20% wt and 10% wt concentration were prepared and stirred for 1 h in chloroform and acetone solvent with 8:2 aspect ratio for applying to shell. PGS was then dissolved chloroform and acetone solvent with 8:2 aspect ratio at a 10% w/v concentration for 30 min for applying to core. To prepare PGS-PRP/PGS-PCL fibers, the PRP was added to PGS solution with 0.5% w/v and mixed for 10 min. Following that, PGS/PGS-PCL and PGS-PRP/PGS-PCL membranes were developed utilizing a coaxial needle (G16 outer diameter (OD) = 1.20 mm and G23 inner diameter (ID) = 0.33 mm). The flow rates of the core and shell, as well as the voltage and tip-to-collector distance, were 0.1 mL/h, 1.5 mL/h, 14 kV, and 16 cm, respectively.

2.5. Materials characterization

2.5.1. Chemical structure

The functional groups of PGS, PCL, PGS/PCL with or without PRP scaffolds was evaluated by Fourier transform infrared spectroscopy (FTIR). The IR beam absorption peaks were observed at a wavelength in the range of 400–4000 cm⁻¹.

2.5.2. Evaluation of fibers morphological

Scanning Electron Microscopy (SEM, Philips, XL30) was used to evaluate morphology, fiber diameters, and porosity of PGS/PCL, PGS-PRP/PCL, PGS/PGS-PCL, and

PGS-PRP/PGS-PCL scaffolds. The specimens were gold sputtered in a vacuum before SEM photography. Following that, Image-J Software (Version 1.52v, USA) selected 20 fibers at random, and their average diameter was calculated. Additionally, the MATLAB Software's evaluation of the porosity percentage [7].

The core and shell of PGS-PRP/PCL and PGS-PRP/PGS-PCL fibers have been seen *via* a transmission electron microscope (TEM). In order to prepare the samples, the fibers were electrospun on a copper grid whose diameter was 2 mm.

2.5.3. Evaluation of water wettability, swelling and degradation

The hydrophilicity of PGS/PCL, PGS-PRP/PCL, PGS/PGS-PCL, and PGS-PRP/PGS-PCL scaffolds was evaluated by placing water drops on each sample using a contact angle meter (XCA-50, PMC, Iran). The average contact angle was measured based on the contact angle values of water drops on at least three points of each sample after 5 s at room temperature ($n=3$).

By immersing electrospun samples ($1 \times 1 \text{ cm}^2$) in a PBS solution (37°C , pH 7.4), the swelling ratio of the PGS/PCL, PGS-PRP/PCL, PGS/PGS-PCL, and PGS-PRP/PGS-PCL samples was evaluated. To achieve this, the items were weighed before being immersed in 5 ml of PBS solution for 24 h. The samples' weight was measured again after being taken out of the PBS solution, and then Equation (1) was used to estimate the swelling rate.:

$$\text{Swelling ratio}(\%) = \frac{W_2 - W_1}{W_1} \times 100 \quad (1)$$

In this equation, W_1 refers to the sample weight when it is dry and W_2 for the sample weight when it is swelled.

For evaluation, the *in vitro* degradation of PGS/PCL, PGS-PRP/PCL, PGS/PGS-PCL, and PGS-PRP/PGS-PCL scaffolds, the scaffolds ($1 \times 1 \text{ cm}^2$) were placed in a 10 mL PBS solution (37°C and pH 7.4). the samples before soaking in PBS weighing and they were immersed in PBS solution during 60 days. Following the samples' removing from the PBS solution and drying, their weight was determined, and using Equation (2), the degradation rate was computed:

$$\text{Degradation ratio}(\%) = \frac{W_1 - W_2}{W_1} \times 100 \quad (2)$$

W_2 represents the sample weight after degradation in time points in this equation, while W_1 represents the sample weight before soaking in PBS.

2.5.4. PRP release behavior

Bradford kit (Parotocib, Iran) is one of the quantitative spectroscopic techniques used to determine the amount of protein (such as PRP proteins) in a solution. The Bovine Serum Albumin (BSA) standard sample was used in this test to develop a standard curve. To account for this, a stock solution of BSA containing $25 \mu\text{g/ml}$ was

developed, and a standard curve has been generated by adding reagent A (a solution of Coomassie Brilliant Blue G-250 dye) to stock solutions at various concentrations (20 μL reagent A + 80 μL standard solution). The sample solution, 10 μL at a time, was then transferred to a well and diluted with water to an ending amount of 80 μL . The wells were subsequently filled with 20 L of reagent A, that was then left to react with the proteins for 5 min. Elisa reader (BioRad 680 Instruments, USA) was used to measure the solutions' absorbance at 595 nm, and the standard curve was utilized to determine the concentration of proteins released at each time point [27,28].

2.5.5. Mechanical behavior and tensile strength of scaffolds

The strength assay was employed to investigate the mechanical properties of PGS/PCL and PGS/PGS-PCL with or without PRP scaffolds. The scaffolds were cut (30 \times 10 \times 1 mm³). According to ASTM D638 standard 10N load cell under a cross-head speed of 10 mm/min was used[29]. The stress-strain curve's linear elastic region's slope was used to calculate the scaffolds' elastic modulus.

2.6. In vitro cell assay

2.6.1. Cell viability

The cell viability of wound dressing membranes with or without PRP has been determined using the MTT test. Samples have been sterilized for this purpose for twenty minutes under UV light. L929 cells obtained from the Cell Bank of the Pasteur Institute for Medical Research in Iran were utilized to evaluate cell viability. At 37°C and 5% CO₂, the L929 cell lines were cultured in DMEM containing 10 v/v% FBS and 1 v/v% streptomycin/penicillin. On both the tissue culture plate (TCP) (control) and the sample plate, 10⁴ cells were added per well. Following that, the samples containing cells were incubated for 5 days, with a 2-day change in the growth medium.

The MTT assay was implemented for examining the cell viability. At days 1, 3, and 5, the culture media was removed, and the cell-seeded samples and control were incubated for 3 h with 100 μL of MTT solution (5 mg/ml). As a result, when the dark blue formazan crystals were dissolved in DMSO, 100 μL of the formazan solution from each sample was transferred to a 96-well plate, and the optical density (OD) was measured against DMSO at a wavelength of 590 nm using a microplate reader (BioRad 680 Instruments, USA). The following equation was used to determine the relative cell survival:

$$\text{Relative cell survival (\% to control)} = \frac{X_s - X_d}{X_t - X_d} \quad (3)$$

Where X_s , X_d and X_t were absorbance of the sample, DMSO as the blank sample and TCP as the control group, respectively.

2.6.2. Cell attachment

Sterilized PGS/PCL, PGS-PRP/PCL, PGS/PGS-PCL, and PGS-PRP/PGS-PCL samples had been placed in each well of a 12-well plate, and 10⁴ cells in 100 μL of the media

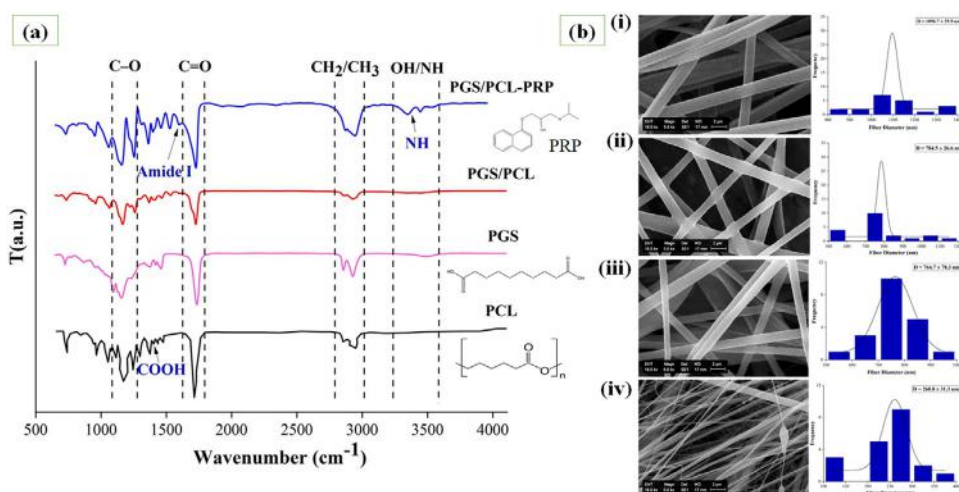


Figure 1. Chemical and morphologies of PGS/PCL and PGS/PCL with and without PRP: (a) FTIR spectra of PGS, PCL, electrospun PGS/PCL and PGS-PRP/PCL scaffolds, and (b) SEM images of coaxial (i) PGS/PCL, (ii) PGS-PRP/PCL, (iii) PGS/PCL, and (iv) PGS-PRP/PCL fibers with fiber diameter size distribution diagrams.

were additionally added on the scaffolds in each well. The samples were then incubated at 37°C with a CO₂ concentration of 5% to examine the cell attachment. The scaffolds were rinsed with PBS and the cell culture media was removed after a period of three days. The cells on the scaffold were subsequently immersed in 2.5 w/v% glutaraldehyde to fix cells. During 4h, the scaffolds were dehydrated with 50%, 60%, 70%, 80%, and 96% ethanol and the glutaraldehyde was removed. The dried scaffolds were covered in a gold coating, and a SEM was used to observe the adhesion of cells to the scaffold surface.

2.7. Statistical analysis

All of the data in this study were analyzed using the one-way ANOVA test. Tukey-Kramer post-hoc test with Origin Software (V.2021) was employed to analyze the statistical significance between the polymers and hydrogels groups, and *p*value < 0.05 was considered statistically significant.

3. Results and discussion

3.1. FTIR analysis

This study presented a coaxial PGS/PCL with or without PRP membrane to accelerate the wound healing. Figure 1a displays the 400–4000cm⁻¹ FTIR spectra of PCL, PGS, coaxial PGS/PCL, and PGS-PRP/PCL. Peaks around 1170cm⁻¹ (C–O), 1728cm⁻¹ (C=O), and 2947cm⁻¹ (C–H group) in the FTIR spectrum belonged to the PCL polymer [29]. Therefore, the peaks around 1159cm⁻¹ and 3448cm⁻¹ were related to the C–O and O–H groups of the PGS polymers [7,30]. These characteristic peaks

Table 1. Fibers diameter and porosity of electrospun membranes.

Coaxial electrospun samples	Fibers diameter (nm)	Porosity (%)
PGS/ PCL	1096.7 ± 29.9	81.33
PGS-PRP/ PCL	784.5 ± 26.6	89.67
PGS/ PGS-PCL	764.7 ± 78.3	83.12
PGS-PRP/ PGS-PCL	260.8 ± 31.3	94.32

demonstrated the combination of the PGS and PCL polymers in the PGS/PCL core-shell electrospun scaffold. After that, the FTIR spectrum of PGS-PRP/PCL displayed a wide band in 1614cm^{-1} and 3458cm^{-1} areas confirmed to amide I and N-H groups from PRP (protein), respectively [31].

3.2. Fibers morphology and structure

The surface morphologies of PGS/PCL, PGS-PRP/PCL, PGS/PGS-PCL, and PGS-PRP/PGS-PCL fibers are shown in Figure 1b. The PGS/PCL (Figure 1b(i)) and PGS-PRP/PCL (Figure 1b(ii)) fibers have regular, uniform, and porous network morphology. In general, PGS is a synthetic polymer that cannot be electrospun alone because of PGS low viscosity [7]. In this study, the PGS can provide electrospun by using the core-shell technique in the core part through PCL polymer as shell fibers. SEM images were used to measure the diameter of 30 fibers, and the distribution of fiber diameter diagram was generated as well. As shown in Table 1, the SEM image of the PGS/PCL group demonstrated that the average diameter of the fibers in this sample is roughly $1096.7 \pm 29.9\text{nm}$. By adding PRP to the core fiber, the diameter of the coaxial electrospun fibers was reduced to $784.5 \pm 26.6\text{nm}$, which has been observed in similar studies [21]. In electrospinning, thinner fibers are produced as a result of the addition of PRP due to their polar properties (the abundant amine groups) [32]. Further, according to other studies, adding PRP to core solution (PGS) may alter the viscosity, surface tension, and interfacial tension between PGS and shell solution (PCL and PGS/PCL). As a result of all these factors, fiber thickness may decrease [33].

In another group, according to Figure 1b(iii) and Figure 1b(iv), by adding PGS in the shell of fibers (PGS/PGS-PCL) and adding PRP to the core of this structure (PGS-PRP/PGS-PCL), the average diameter of PGS/PCL fibers was reduced to $764.7 \pm 78.3\text{nm}$ and $260.8 \pm 31.3\text{nm}$, respectively (Table 1). It seems that by adding PRP to PGS/PGS-PCL, the stretch of fibers in the electric field become easier and fibers adapt to nanostructure. Whereas PGS is added to the shell, the viscosity of the solution decreases, as decreases the diameter of the fibers. It is well-known that the electrical conductivity and viscosity of the solution influence the morphology and diameter of fibers created *via* the electrospinning technique. Both of these factors can be changed in order to generate perfect fibers with uniform structures [33,34].

Optimizing the scaffold porosity for cell proliferation and migration is a significant challenge when designing tissue engineering scaffolds [35]. The porosity of the skin facilitates the formation of the ECM and improves cell migration and skin regeneration [36]. As shown in Table 1, the porosity of PGS/PCL, PGS-PRP/PCL, PGS/PGS-PCL, and PGS-PRP/PGS-PCL core-shell fibrous scaffolds were approximately 81.33%, 89.67%, 83.12%, and 94.32%, respectively. In fact, by adding PRP to the fiber

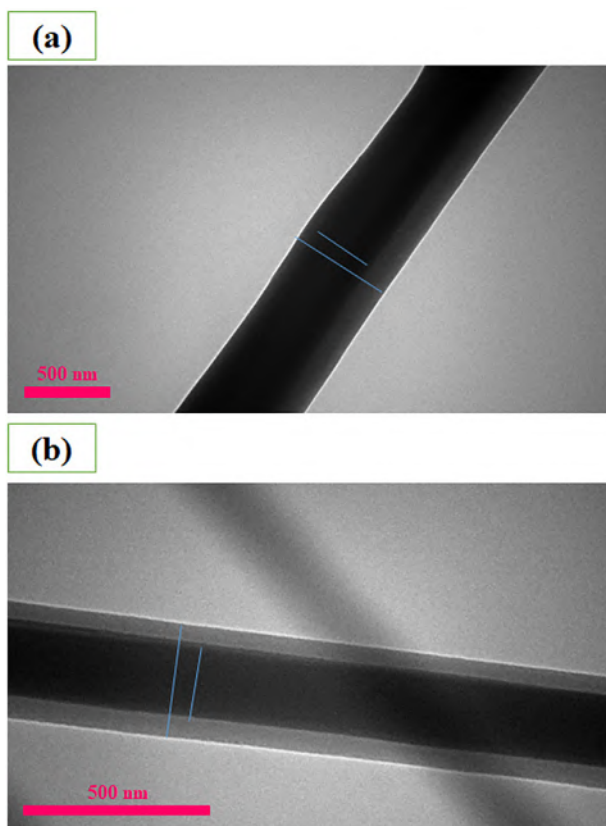


Figure 2. TEM image of coaxial (a) PGS-PRP/PCL and (b) PGS-PRP/PGS-PCL fibers.

structure and decreasing fiber diameters, the porosity increased. The porosity of membranes is an essential parameter in the wound healing process and high permeability, as well as nutrients and oxygen distribution [37]. Previous research concluded that the best percentage of surface porosity for skin tissue engineering was around 85%, providing the conditions for an ideal surface for skin cell interaction [17]. The current study demonstrated that the PGS/PGS-PCL containing PRP by nanostructure and high porosity can be best sample in comparison with other samples to improve cell reaction. In a similar study, Chen et al. [33] found that adding PRP to fiber cores (hyaluronic acid) and changing solution viscosity leads to larger pores in final scaffolds.

Figure 2 shows the TEM images of PGS-PRP/PCL (Figure 2a) and PGS-PRP/PGS-PCL (Figure 2b) core-shell samples after evaluation of fiber morphology. PGS-PRP corresponds to the inner dark regions of the nanofiber. TEM images demonstrate that a core-shell structure formed in a nanofiber whose core layer was darker than its shell layer. There is a contrast between the core and shell layers of fiber due to the difference in electron beam transmissibility between PGS and PCL regions. As shown in Figure 2, in both PGS-PRP/PCL and PGS-PRP/PGS-PCL samples, it can be said that the thickness of the core area is approximately 70% of the total diameter of a fibers. For example, in the PGS-PRP/PCL membrane, the fiber

diameter was 750 ± 23 nm, the thickness of the core region was 530 ± 20 nm. This represented the various phenomenon of the core, showing that the volume of the core was more than that which could be stretched by viscous drag forces from the shell [38]. The physical, mechanical properties, and especially the drug release behavior enhanced by increasing the diameter of the fiber core compared to the shell [39].

3.3. Evaluation of water contact angle and swelling evaluations

Hydrophilicity plays a major role in the interaction between biomaterials and cells [40]. For instance, super hydrophilic or hydrophobic surfaces are unsuitable for supporting cell viability and attachment [12]. Figure 3a shows the water contact angles for PGS/PCL, PGS-PRP/PCL, PGS/PGS-PCL, and PGS-PRP/PGS-PCL nanofiber scaffolds and indicates that their water contact angles were $63.66^\circ \pm 2$, $54^\circ \pm 3$, $47.33^\circ \pm 5$, and $32.66^\circ \pm 3$, respectively. By adding PGS and PRP to PCL in nanofibers, the water contact angle decreased significantly. It is due to hydrophilic OH groups of PGS and amine functional groups of PRP. In other words, by adding hydrophilic PGS and PRP to the polymer structure, the interaction between polymers nanofibers and water molecules was increased and, as a result, enhanced hydrophilicity. Also, decreasing the fiber diameter and thus increasing the specific surface area can be a reason for increasing the hydrophilicity of PGS-PRP/PCL and PGS-PRP/PGS-PCL nanofibers compared to other samples. According to previous studies, the proper wettability for skin cell attachment was around $30\text{--}40^\circ$ [41]. This study showed that the PGS-PRP/PGS-PCL with a contact angle around 32° could be ideal for cells skin interaction.

The ideal wound dressing should absorb exudate from the wound and prevent it from accumulating at the wound site and prevent wound dehydration [42]. The swelling ratio for various samples is shown in Figure 3b. The PGS-PRP/PCL fiber swelling ratio was $168.53 \pm 12\%$, higher than PGS/PCL sample ($\sim 138 \pm 9\%$). It may be caused by the hydrophilic functional groups present in PRP. Consequently, the PGS-PRP/PGS-PCL

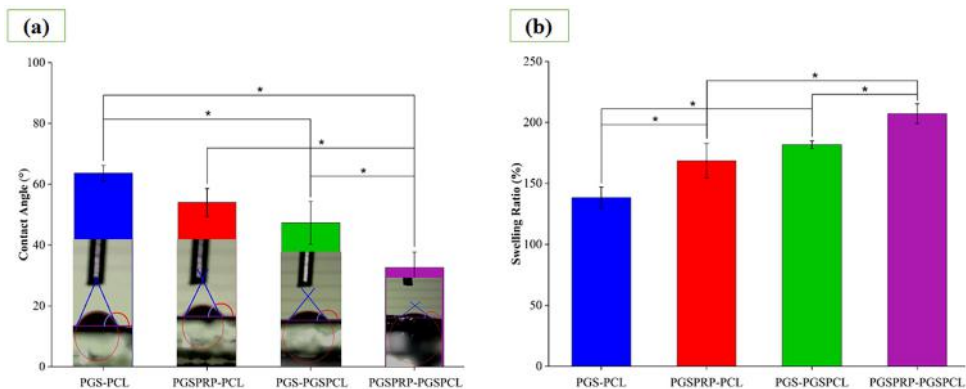


Figure 3. Physical evaluation of PGS/PCL, PGS-PRP/PCL, PGS/PGS-PCL and PGS-PRP/PGS-PCL: (a) contact angle of coaxial samples, and (b) the mass swelling ratio after 24h drenching in PBS solution at 37°C . All values are characterized as corresponding to the averages ($n=3$) \pm standard deviation (*: $p < 0.05$).

fiber scaffold showed a swelling ratio of $\sim 207.19 \pm 8\%$, which is higher than the sample without platelet-rich plasma ($\sim 181 \pm 4\%$). The results of the water absorption and the water measurement of contact angle were in conformity. This level of hydrophilicity and the presence of hydrophilic functional groups, such as amines and OH, in a sample influence the rate that it swells. [43]. The swelling rate in PGS-PRP/PGS-PCL is in the appropriate range for absorbing wound exudate [44].

3.4. In vitro degradation

The degradation process of polymer related to molecular weight, hydrophilicity, porosity, crystallinity, and the type of polymer material [45]. In Figure 4a, fiber scaffolds made of PGS/PCL, PGS-PRP/PCL, PGS/PGS-PCL, and PGS-PRP/PGS-PCL were investigated for 60 days following immersion in PBS. The different degradability processes occurred for four groups of samples during this period. As shown in Figure 4a, there were significant differences between the degradation process of PGS/PCL and PGS/PGS-PCL fibers during 60 days due to hydrolytic degradation of PGS in the shell of fibers. In other words, PGS/PGS-PCL and PGS/PCL membranes exhibited nearly linear degradation profile and PGS/PGS-PCL followed the highest weight loss compared to PGS/PCL scaffolds. The reason for the fast degradation rate of PGS scaffolds may be the hydrolysis of the ester bonds in PGS blends in the shell of fibers [46]. As the PCL is alone in the shell, the degradation rate of PGS/PCL scaffolds significantly decreased. Despite all these changes in the weight of the wound dressing (PGS/PCL, PGS-PRP/PCL, PGS/PGS-PCL, and PGS-PRP/PGS-PCL), scaffolds had maintained their integrity during 60 days. Similarly, Shilpa et al. [47] evaluated the mechanical and degradation behavior of the PGS/PCL scaffold. Their results demonstrated that by adding and increasing PGS concentration, the hydrolytic degradation accelerated compared to PCL scaffolds. Furthermore, our study showed that no significant difference occurred between degradation profiles by adding PRP to PGS/PCL and PGS/PGS-PCL structure ($p > 0.05$).

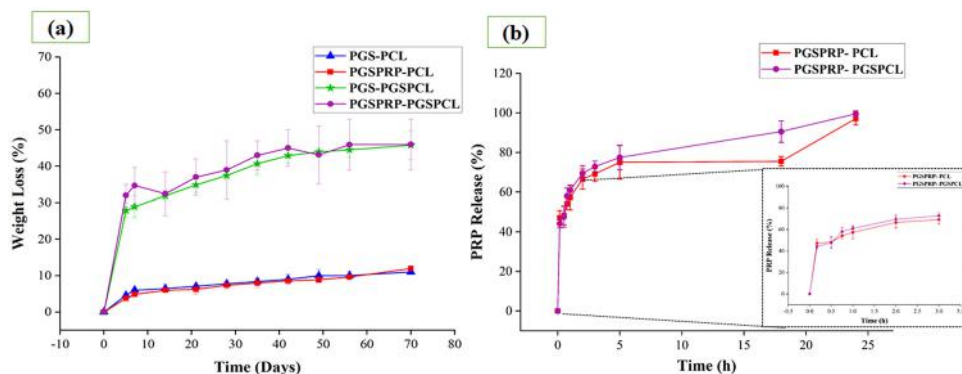


Figure 4. (a) *In vitro* degradation evaluation of PGS/PCL, PGS-PRP/PCL, PGS/PGS-PCL and PGS-PRP/PGS-PCL after 60 days soaking in PBS solution at 37°C, and (b) release profiles of PRP from PGS-PRP/PCL and PGS-PRP/PGS-PCL coaxial scaffolds in PBS solution at 37°C. All values are characterized as corresponding to the averages ($n=3$) \pm standard deviation.

3.5. PRP release of PGS/PCL and PGS/PGS-PCL scaffolds

In this study, PRP was loaded within the core of PGS/PCL and PGS/PGS-PCL scaffolds using coaxial electrospinning. The release of PRP from PGS/PCL and PGS/PGS-PCL scaffolds was evaluated for one day. In [Figure 4b](#), the cumulative PRP release profile from PGS-PRP/PCL and PGS-PRP/PGS-PCL scaffolds after three hours was measured to be 69% and 72%, respectively. This burst release of PRP is due to the rapid interaction of water molecules with the amide part of this biological compound and the cumulative delivery of small protein molecules of PRP from the scaffold structure [48,49]. Another reason for the fast PRP release was the high volume ratio of the core to the shell of the fibers, as shown in [Figure 2](#). This issue leads to increasing the probability of the contact surface with water molecules and burst release of PRP [50].

In the present work, during five hours, the PGS-PRP/PCL was compared to PGS-PRP/PGS-PCL following sustained release due to the hydrophobic structure of PCL. In other words, water molecules need time to penetrate the structure of the scaffold. Also, by adding PGS to the shell and increasing the swelling ratio and more PBS penetration, burst release occurred in PGS-PRP/PGS-PCL during 24h. Approximately 90% of PRP was released from PGS-PRP/PCL, and 98% from PGS-PRP/PGS-PCL nanofibrous scaffold during one day. Similarly, Gomez et al. [21] evaluated the released PRP of PCL/PRP scaffolds and demonstrated that more VEGF and PRP proteins were released during four hours. Therefore, the PRP release rate of PGS-PRP/PGS-PCL can be suitable for skin tissue engineering applications.

3.6. Mechanical properties of scaffolds

Strength and flexibility are important mechanical properties for an ideal wound dressing [51]. A wound dressing must be sufficiently strong for protecting against external forces while still being flexible enough to avoid damaging the underlying tissues during movement [52]. Meanwhile, favorable mechanical properties are essential for stimulating cell growth and differentiation. The chemical composition of fibers, average fiber diameter, morphology, and uniformity of fibers affect the mechanical properties of electrospun samples [17]. This study investigated the stress-strain behavior, tensile strength, elongation, and young modulus of PGS/PCL, PGS-PRP/PCL, PGS/PGS-PCL and PGS-PRP/PGS-PCL prepared scaffolds ([Figure 5a-d](#)).

The results showed that the PGS/PCL scaffolds followed the highest stress strength, elastic modulus, and elongation value. According to the tensile assay result, elongation was decreased by adding PRP to core of the samples. A similar trend was observed for tensile strength, as shown in [Figure 5b](#), that by adding PRP to the scaffolds, the tensile strength was decreased (~2 times). Interestingly, the young modulus of PGS/PCL and PGS/PGS-PCL scaffolds were evaluated 5.17 ± 0.7 MPa and 2.71 ± 0.3 MPa, respectively. Similarly, Silva et al. [53] evaluated the effect of PGS concentration on the mechanical properties of coaxial PGS/PCL-Kartogenin nanofibers for cartilage tissue engineering. This study demonstrated that by adding PGS to fiber and decreasing the fiber diameters, the tensile strength and stiffness were

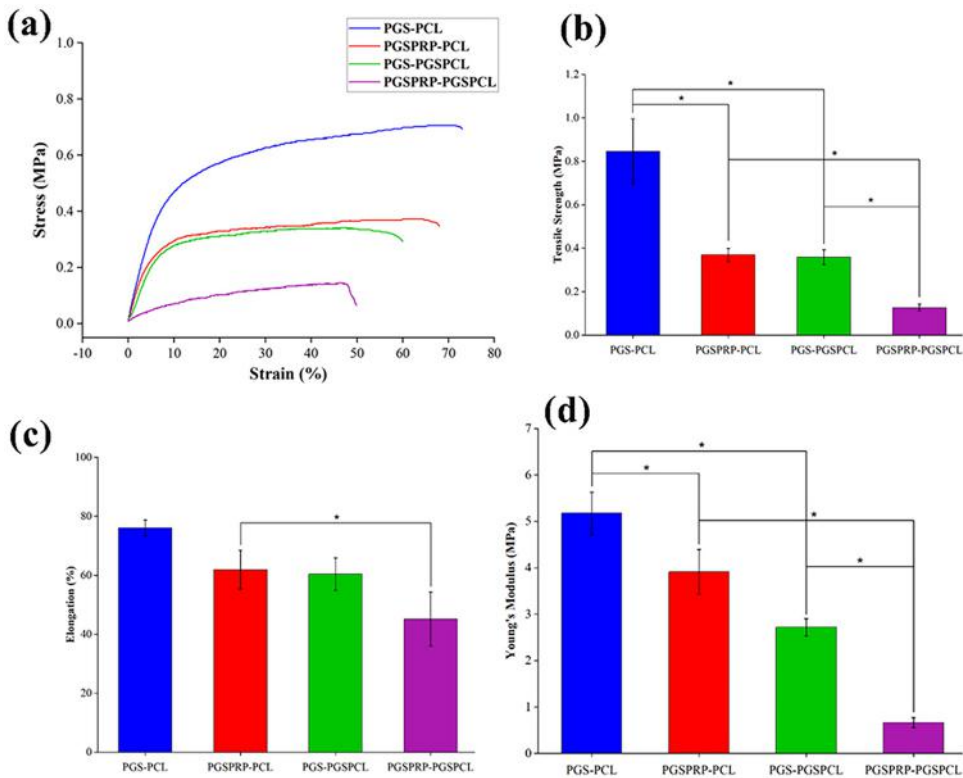


Figure 5. Mechanical characteristics of PGS/PCL, PGS-PRP/PCL, PGS/PGS-PCL and PGS-PRP/PGS-PCL: (a) stress-strain curves, (b) tensile strength, (c), elongation and (d) elastic modulus of samples. All values are characterized as corresponding to the averages ($n=3$) \pm standard deviation. (*: $p < 0.05$).

reduced. As shown in Figure 1b and Table 1, loading PRP to the core and adding PGS to the shell of fibers resulted in changes in the fiber morphology and diameter, which play an essential role in determining the mechanical properties of electrospun scaffolds.

Previous studies demonstrated that the tensile and elongation properties were reduced by increasing the percentage of porosity [54]. Kim et al. [55] showed that PCL mats with larger average fiber diameters (more than 0.8 μ m) showed superior extensibility and demonstrated that fiber morphology (including average fiber size) of electrospun membrane is significantly related to mechanical properties. According to the present study, when PRP was added to the core and fiber diameters were decreased, the elongation was significantly reduced. It appears that fiber morphology (including average fiber size) of electrospun membraned mats is significantly related to mechanical properties, despite the exact relationship still being unclear.

However, Kong et al. [56] demonstrated that the suitable young modulus for wound dressing is 0.5–2 MPa. Therefore, according to the mechanical and physical properties, it can be concluded that the PGS-PRP/PGS-PCL is a suitable candidate for biological evaluation for skin tissue engineering applications.

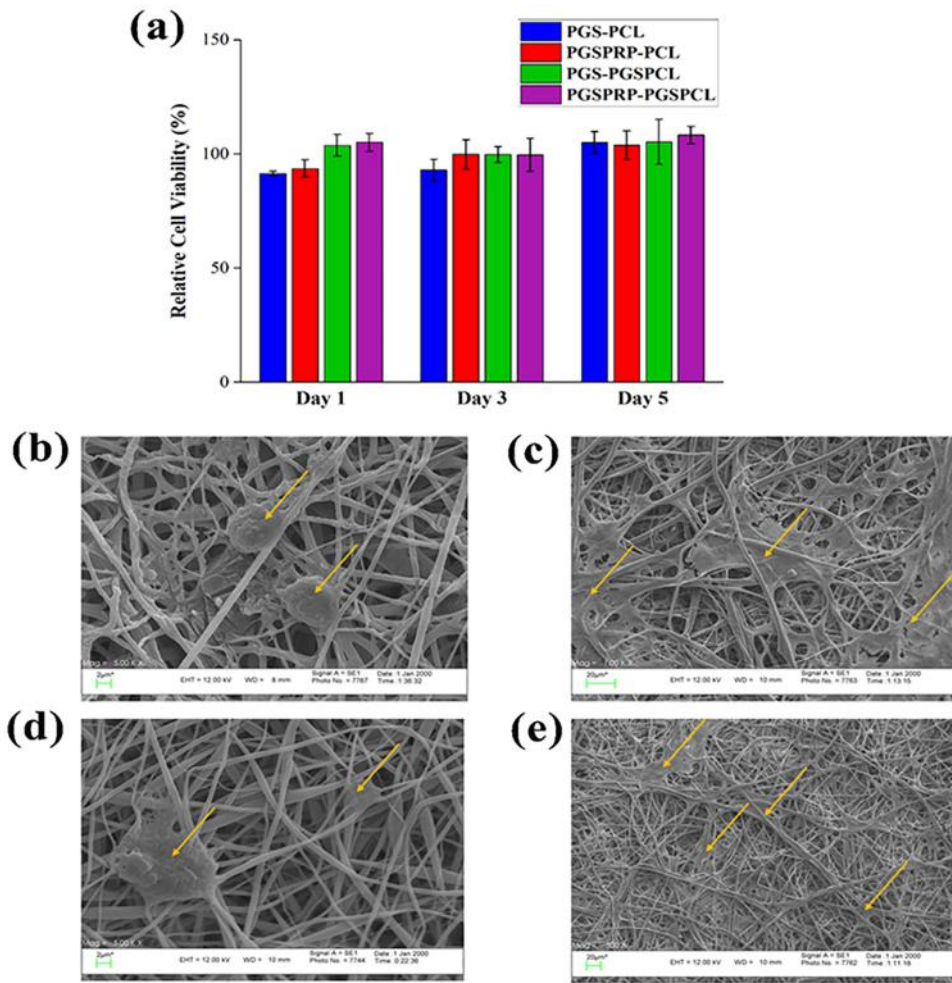


Figure 6. The viability of cells and the attachment of cells to scaffolds. (a) Evaluation of the viability of L929 cells seeded on PGS/PCL, PGS-PRP/PCL, PGS/PGS-PCL, PGS-PRP/PGS-PCL scaffolds, as well as a control sample (TCP), and representative SEM images of L929 cell adhesion to the scaffold surfaces after 3 days of culture on (b) PGS/PCL, (c) PGS-PRP/PCL, (d) PGS/PGS-PCL, and (e) PGS-PRP/PGS-PCL scaffolds. All values are characterized as corresponding to the averages ($n=3$) \pm standard deviation. (*: $p<0.05$).

3.7. In vitro cell viability and cell attachment

In order to determine the scaffolds' biocompatibility, we used MTT assay and cell adhesion by employing L929 cells to determine the viability, proliferation, adhesion, and spreading of cells (Figure 6). The effect of PRP in the core layer of PGS/PCL and PGS/PGS-PCL scaffolds on cell survival was investigated in this work. When compared to TCP, L929 cell viability on the surface of PGS/PCL, PGS-PRP/PCL, PGS/PGS-PCL, and PGS-PRP/PGS-PCL core-shell scaffolds is shown in Figure 6a. For PGS/PCL, PGS-PRP/PCL, PGS/PGS-PCL, and PGS-PRP/PGS-PCL samples during five days, the viability was $105.08 \pm 3\%$, $103.92 \pm 5\%$, $105.36 \pm 2\%$, and $108.3 \pm 3\%$, respectively. Despite this, there was no noticeable difference in relative cell viability

between scaffolds. According to cell viability results, all scaffolds had suitable cell compatibility and no toxicity for skin cells.

Figures 6b–e show the spreading and adhesion of cells on the surface of samples. Due to the PRP addition to the core of fibers in PGS-PRP/PCL (Figure 6c) and PGS-PRP/PGS-PCL (Figure 6e), by increasing the surface area and porosity as compared to PGS/PCL and PGS/PGS-PCL, increasing cell proliferation and attachment to core-shell scaffolds occurred. Similarly, Movahedi et al. [57] demonstrated that high porosity in the structure helps exchange oxygen and nutrients materials and improves conditions for cell adhesion. On the other hand, more hydrophilic groups in PGS-PRP/PCL and PGS-PRP/PGS-PCL and their counterpart without PRP improved cell attachment and proliferation for scaffolds [58]. PRP and its growth factors can also cause cell migration, proliferation, and skin tissue regeneration in PGS-PRP/PCL and PGS-PRP/PGS-PCL scaffolds [59]. However, according to the SEM images, PGS-PRP/PGS-PCL demonstrated better cellular behavior.

4. Conclusion

In conclusion, we successfully fabricated a PGS/PCL and PGS/PGS-PCL with and without PRP coaxial fibers to promote wound healing. The obtained scaffolds presented the core-shell structure, suitable swelling capacity, degradation profile, and tunable mechanical and biological properties. By adding PRP to scaffolds, the swelling, degradation ratio, and mechanical behavior would display different profiles. PGS-PRP/PCL and PGS-PRP/PGS-PCL wound dressing demonstrated their superior bio function by enhancing the biocompatibility and adhesion of L929 cells. Collectively, it has been proven that core-shell nanofibers are an effective wound dressing that can promote wound healing by releasing PRP at the wound site. In this study, the fabricated PGS/PCL and PGS/PGS-PCL containing PRP scaffold with suitable release of PRP could be a potent wound dressing for enhanced skin wound repair.

Disclosure statement

No potential conflict of interest was reported by the author(s).

Funding

The authors acknowledge the financial support of Isfahan University of Medical Sciences through grant [No. #398819].

ORCID

Anousheh Zargar Kharazi  <http://orcid.org/0000-0001-8945-0144>

References

- [1] Biglari S, Le TYL, Tan RP, et al. Simulating inflammation in a wound microenvironment using a dermal wound-on-a-chip model. *Adv Healthc Mater.* 2019;8:1801307.

- [2] Barros NR, Kim H-J, Goudie MJ, et al. Biofabrication of endothelial cell, dermal fibroblast, and multilayered keratinocyte layers for skin tissue engineering. *Biofabrication*. 2021;13(3):035030. doi: [10.1088/1758-5090/aba503](https://doi.org/10.1088/1758-5090/aba503).
- [3] Bello YM, Phillips TJ. Recent advances in wound healing. *Jama*. 2000;283(6):716–718. doi: [10.1001/jama.283.6.716](https://doi.org/10.1001/jama.283.6.716).
- [4] Adeli H, Khorasani MT, Parvazinia M. Wound dressing based on electrospun PVA/chitosan/starch nanofibrous mats: fabrication, antibacterial and cytocompatibility evaluation and in vitro healing assay. *Int J Biol Macromol*. 2019;122:238–254. doi: [10.1016/j.ijbiomac.2018.10.115](https://doi.org/10.1016/j.ijbiomac.2018.10.115).
- [5] Heydari P, Kharaziha M, Varshosaz J, et al. Current knowledge of immunomodulation strategies for chronic skin wound repair. *J Biomed Mater Res*. 2021;110(2):265–288. doi: [10.1002/jbm.b.34921](https://doi.org/10.1002/jbm.b.34921).
- [6] Amini F, Semnani D, Karbasi S, et al. A novel bilayer drug-loaded wound dressing of PVDF and PHB/chitosan nanofibers applicable for post-surgical ulcers. *Int J Polym Mater Polym Biomater*. 2019;68(13):772–777. doi: [10.1080/00914037.2018.1506982](https://doi.org/10.1080/00914037.2018.1506982).
- [7] Heydari P, Varshosaz J, Zargar Kharazi A, et al. Preparation and evaluation of poly glycerol sebacate/poly hydroxy butyrate core-shell electrospun nanofibers with sequentially release of ciprofloxacin and simvastatin in wound dressings. *Polym Adv Technol*. 2018;29(6):1795–1803. doi: [10.1002/pat.4286](https://doi.org/10.1002/pat.4286)
- [8] Movahedi M, Karbasi S. A core-shell electrospun scaffold of polyhydroxybutyrate-starch/halloysite nanotubes containing extracellular matrix and chitosan for articular cartilage tissue engineering application. *J Polym Environ*. 2023;31:3052–3069. doi: [10.1007/s10924-023-02800-6](https://doi.org/10.1007/s10924-023-02800-6)
- [9] Heydari P, Zargar Kharazi A, Asgary S, et al. Comparing the wound healing effect of a controlled release wound dressing containing curcumin/ciprofloxacin and simvastatin/ciprofloxacin in a rat model: a preclinical study. *J Biomed Mater Res Part A*. 2021; 110(2):341-352. doi: [10.1002/jbm.a.37292](https://doi.org/10.1002/jbm.a.37292).
- [10] Su S, Bedir T, Kalkandelen C, et al. Coaxial and emulsion electrospinning of extracted hyaluronic acid and keratin based nanofibers for wound healing applications. *Eur Polym J*. 2021;142:110158. doi: [10.1016/j.eurpolymj.2020.110158](https://doi.org/10.1016/j.eurpolymj.2020.110158).
- [11] Fakhrali A, Semnani D, Salehi H, et al. Electrospun PGS/PCL nanofibers: from straight to sponge and spring-like morphology. *Polym Adv Technol*. 2020;31(12):3134–3149. doi: [10.1002/pat.5038](https://doi.org/10.1002/pat.5038).
- [12] Luginina M, Schuhlraden K, Orrú R, et al. Electrospun PCL/PGS composite fibers incorporating bioactive glass particles for soft tissue engineering applications. *Nanomaterials*. 2020;10(5):978. doi: [10.3390/nano10050978](https://doi.org/10.3390/nano10050978).
- [13] Ghafarzadeh M, Kharaziha M, Atapour M, et al. Copper-chitosan nanoparticles incorporated PGS/MAO bilayer coatings for potential cardiovascular application. *Prog Org Coatings*. 2023;174:107269. doi: [10.1016/j.porgcoat.2022.107269](https://doi.org/10.1016/j.porgcoat.2022.107269).
- [14] Frydrych M, Román S, MacNeil S, et al. Biomimetic poly (glycerol sebacate)/poly (L-lactic acid) blend scaffolds for adipose tissue engineering. *Acta Biomater*. 2015;18:40–49. doi: [10.1016/j.actbio.2015.03.004](https://doi.org/10.1016/j.actbio.2015.03.004).
- [15] Karbasi S, Hashemibeni B, Honarvar A, et al. PCL/agarose 3D-printed scaffold for tissue engineering applications: fabrication, characterization, and cellular activities. *Res Pharm Sci*. 2023;18(5):566–579. doi: [10.4103/1735-5362.383711](https://doi.org/10.4103/1735-5362.383711).
- [16] Franco RA, Nguyen TH, Lee BT. Preparation and characterization of electrospun PCL/PLGA membranes and chitosan/gelatin hydrogels for skin bioengineering applications. *J Mater Sci Mater Med*. 2011;22(10):2207–2218. doi: [10.1007/s10856-011-4402-8](https://doi.org/10.1007/s10856-011-4402-8).
- [17] Salehi M, Niyakan M, Ehterami A, et al. Porous electrospun poly(ϵ -caprolactone)/gelatin nanofibrous mat containing cinnamon for wound healing application: in vitro and in vivo study. *Biomed Eng Lett*. 2020;10(1):149–161. doi: [10.1007/s13534-019-00138-4](https://doi.org/10.1007/s13534-019-00138-4).
- [18] Zadehnajar P, Karbasi S, Akbari B, et al. Incorporation of multi-walled carbon nanotubes into electrospun PCL/gelatin scaffold: the influence on the physical, chemical and

- thermal properties and cell response for tissue engineering. *Mater Technol.* 2020;35(1): 39–49. doi: [10.1080/10667857.2019.1651539](https://doi.org/10.1080/10667857.2019.1651539).
- [19] Ehterami A, Salehi M, Farzamfar S, et al. In vitro and in vivo study of PCL/COLL wound dressing loaded with insulin-chitosan nanoparticles on cutaneous wound healing in rats model. *Int J Biol Macromol.* 2018;117:601–609. doi: [10.1016/j.ijbiomac.2018.05.184](https://doi.org/10.1016/j.ijbiomac.2018.05.184).
- [20] Dimatteo R, Darling NJ, Segura T. In situ forming injectable hydrogels for drug delivery and wound repair. *Adv Drug Deliv Rev.* 2018;127:167–184. doi: [10.1016/j.addr.2018.03.007](https://doi.org/10.1016/j.addr.2018.03.007).
- [21] Diaz-Gomez L, Alvarez-Lorenzo C, Concheiro A, et al. Biodegradable electrospun nanofibers coated with platelet-rich plasma for cell adhesion and proliferation. *Mater Sci Eng C Mater Biol Appl.* 2014;40:180–188. doi: [10.1016/j.msec.2014.03.065](https://doi.org/10.1016/j.msec.2014.03.065).
- [22] Samadian H, Ehterami A, Sarrafzadeh A, et al. Sophisticated polycaprolactone/gelatin nanofibrous nerve guided conduit containing platelet-rich plasma and citicoline for peripheral nerve regeneration: in vitro and in vivo study. *Int J Biol Macromol.* 2020;150: 380–388. doi: [10.1016/j.ijbiomac.2020.02.102](https://doi.org/10.1016/j.ijbiomac.2020.02.102).
- [23] Zhang X, Yao D, Zhao W, et al. Engineering platelet-rich plasma based dual-network hydrogel as a bioactive wound dressing with potential clinical translational value. *Adv Funct Mater.* 2021;31:2009258.
- [24] Shi L, Lin F, Zhou M, et al. Preparation of biocompatible wound dressings with dual release of antibiotic and platelet-rich plasma for enhancing infected wound healing. *J Biomater Appl.* 2021;36(2):219–236. doi: [10.1177/0885328221996013](https://doi.org/10.1177/0885328221996013).
- [25] Rai R, Tallawi M, Grigore A, et al. Synthesis, properties and biomedical applications of poly(glycerol sebacate) (PGS): a review. *Prog Polym Sci.* 2012;37(8):1051–1078. doi: [10.1016/j.progpolymsci.2012.02.001](https://doi.org/10.1016/j.progpolymsci.2012.02.001).
- [26] Dashore S, Chouhan K, Nanda S, et al. Preparation of platelet-rich plasma: national IADVL PRP taskforce recommendations. *Indian Dermatol Online J.* 2021;12(Suppl 1): S12–S23. doi: [10.4103/idoj.idoj_269_21](https://doi.org/10.4103/idoj.idoj_269_21).
- [27] Zhang Y, Wang X, Chen J, et al. Exosomes derived from platelet-rich plasma administration in site mediate cartilage protection in subtalar osteoarthritis. *J Nanobiotechnology.* 2022;20(1):56. doi: [10.1186/s12951-022-01245-8](https://doi.org/10.1186/s12951-022-01245-8).
- [28] Abazari MF, Nejati F, Nasiri N, et al. Platelet-rich plasma incorporated electrospun PVA-chitosan-HA nanofibers accelerates osteogenic differentiation and bone reconstruction. *Gene.* 2019;720:144096. doi: [10.1016/j.gene.2019.144096](https://doi.org/10.1016/j.gene.2019.144096).
- [29] Karizmeh MS, Poursamar SA, Kefayat A, et al. An in vitro and in vivo study of PCL/chitosan electrospun mat on polyurethane/propolis foam as a bilayer wound dressing. *Mater Sci Eng C Mater Biol Appl.* 2022;135:112667. doi: [10.1016/j.msec.2022.112667](https://doi.org/10.1016/j.msec.2022.112667).
- [30] Kharaziha M, Nikkhah M, Shin S-R, et al. PGS: gelatin nanofibrous scaffolds with tunable mechanical and structural properties for engineering cardiac tissues. *Biomaterials.* 2013;34(27):6355–6366. doi: [10.1016/j.biomaterials.2013.04.045](https://doi.org/10.1016/j.biomaterials.2013.04.045).
- [31] Tang Y, Zhang H, Wei Q, et al. Biocompatible chitosan–collagen–hydroxyapatite nanofibers coated with platelet-rich plasma for regenerative engineering of the rotator cuff of the shoulder. *RSC Adv.* 2019;9(46):27013–27020. doi: [10.1039/c9ra03972d](https://doi.org/10.1039/c9ra03972d).
- [32] Solovieva AO, Permyakova ES, Ershov KI, et al. Plasma-coated PCL scaffolds with immobilized platelet-rich plasma enhance the wound healing in diabetics mice. *Plasma Process Polym.* 2022;19(7):e2200032. doi: [10.1002/ppap.202200032](https://doi.org/10.1002/ppap.202200032).
- [33] Chen C-H, Chen S-H, Chen S-H, et al. Hyaluronic acid/platelet rich plasma-infused core-shell nanofiber membrane to prevent postoperative tendon adhesion and promote tendon healing. *Int J Biol Macromol.* 2023;231:123312. doi: [10.1016/j.ijbiomac.2023.123312](https://doi.org/10.1016/j.ijbiomac.2023.123312).
- [34] Li Y, Li J, Soria RB, et al. Aramid nanofiber and modified ZIF-8 constructed porous nanocomposite membrane for organic solvent nanofiltration. *J Memb Sci.* 2020;603:118002. doi: [10.1016/j.memsci.2020.118002](https://doi.org/10.1016/j.memsci.2020.118002).

- [35] Buenzli PR, Lanaro M, Wong CS, et al. Cell proliferation and migration explain pore bridging dynamics in 3D printed scaffolds of different pore size. *Acta Biomater.* 2020; 114:285–295. doi: [10.1016/j.actbio.2020.07.010](https://doi.org/10.1016/j.actbio.2020.07.010).
- [36] Zhu X, Cui W, Li X, et al. Electrospun fibrous mats with high porosity as potential scaffolds for skin tissue engineering. *Biomacromolecules.* 2008;9(7):1795–1801. doi: [10.1021/bm800476u](https://doi.org/10.1021/bm800476u).
- [37] Xia J, Zhang H, Yu F, et al. Superclear, porous cellulose membranes with chitosan-coated nanofibers for visualized cutaneous wound healing dressing. *ACS Appl Mater Interfaces.* 2020;12(21):24370–24379. doi: [10.1021/acsami.0c05604](https://doi.org/10.1021/acsami.0c05604).
- [38] Haghghat F, Hosseini Ravandi SA, Nasr Esfahany M, et al. A comprehensive study on optimizing and thermoregulating properties of core-shell fibrous structures through coaxial electrospinning. *J Mater Sci.* 2018;53(6):4665–4682. doi: [10.1007/s10853-017-1856-1](https://doi.org/10.1007/s10853-017-1856-1).
- [39] Li M, Zheng Y, Xin B, et al. Coaxial electrospinning: jet motion, core-shell fiber morphology, and structure as a function of material parameters. *Ind Eng Chem Res.* 2020;59(13):6301–6308. doi: [10.1021/acs.iecr.9b05866](https://doi.org/10.1021/acs.iecr.9b05866).
- [40] Roy N, Saha N, Kitano T, et al. Development and characterization of novel medicated hydrogels for wound dressing. *Soft Mater.* 2010;8(2):130–148. doi: [10.1080/15394451003756282](https://doi.org/10.1080/15394451003756282).
- [41] Arima Y, Iwata H. Effect of wettability and surface functional groups on protein adsorption and cell adhesion using well-defined mixed self-assembled monolayers. *Biomaterials.* 2007;28(20):3074–3082. doi: [10.1016/j.biomaterials.2007.03.013](https://doi.org/10.1016/j.biomaterials.2007.03.013).
- [42] Elsayed RE, Madkour TM, Azzam RA. Tailored-design of electrospun nanofiber cellulose acetate/poly(lactic acid) dressing mats loaded with a newly synthesized sulfonamide analog exhibiting superior wound healing. *Int J Biol Macromol.* 2020;164:1984–1999. doi: [10.1016/j.ijbiomac.2020.07.316](https://doi.org/10.1016/j.ijbiomac.2020.07.316).
- [43] Heydari P, Parham S, Kharazi AZ, et al. In vitro comparison study of plasma treated bilayer PGS/PCL and PGS/PLA scaffolds for vascular tissue engineering. *Fibers Polym.* 2022;23(9):2384–2393. doi: [10.1007/s12221-022-0228-x](https://doi.org/10.1007/s12221-022-0228-x).
- [44] Ye P, Wei S, Luo C, et al. Long-term effect against methicillin-resistant staphylococcus aureus of emodin released from coaxial electrospinning nanofiber membranes with a biphasic profile. *Biomolecules.* 2020;10(3):362. doi: [10.3390/biom10030362](https://doi.org/10.3390/biom10030362).
- [45] Yang B, Wang S, Ding M, et al. Hierarchical structure and properties of high-density polyethylene (HDPE) microporous films fabricated via thermally-induced phase separation (TIPS): effect of presence of ultra-high molecular weight polyethylene (UHMWPE). *Polym Adv Technol.* 2022;33(10):3125–3136. doi: [10.1002/pat.5765](https://doi.org/10.1002/pat.5765).
- [46] Wu Z, Li Q, Wang L, et al. A novel biomimetic nanofibrous cardiac tissue engineering scaffold with adjustable mechanical and electrical properties based on poly (glycerol sebacate) and polyaniline. *Mater Today Bio.* 2023;23:100798. doi: [10.1016/j.mtbio.2023.100798](https://doi.org/10.1016/j.mtbio.2023.100798).
- [47] Sant S, Iyer D, Gaharwar AK, et al. Effect of biodegradation and de novo matrix synthesis on the mechanical properties of valvular interstitial cell-seeded polyglycerol sebacate-polycaprolactone scaffolds. *Acta Biomater.* 2013;9(4):5963–5973. doi: [10.1016/j.actbio.2012.11.014](https://doi.org/10.1016/j.actbio.2012.11.014).
- [48] Kamaly N, Yameen B, Wu J, et al. Degradable controlled-release polymers and polymeric nanoparticles: mechanisms of controlling drug release. *Chem Rev.* 2016;116(4):2602–2663. doi: [10.1021/acs.chemrev.5b00346](https://doi.org/10.1021/acs.chemrev.5b00346).
- [49] Jain E, Chinzei N, Blanco A, et al. Platelet-rich plasma released from polyethylene glycol hydrogels exerts beneficial effects on human chondrocytes. *J Orthop Res.* 2019; 37(11):2401–2410. doi: [10.1002/jor.24404](https://doi.org/10.1002/jor.24404).
- [50] Abdullah MF, Nuge T, Andriyana A, et al. Core-shell fibers: design, roles, and controllable release strategies in tissue engineering and drug delivery. *Polymers.* 2019;11(12):2008. doi: [10.3390/polym11122008](https://doi.org/10.3390/polym11122008).

- [51] Lin WC, Lien CC, Yeh HJ, et al. Bacterial cellulose and bacterial cellulose-chitosan membranes for wound dressing applications. *Carbohydr Polym.* 2013;94(1):603–611. doi: [10.1016/j.carbpol.2013.01.076](https://doi.org/10.1016/j.carbpol.2013.01.076).
- [52] Zahiri M, Khanmohammadi M, Goodarzi A, et al. Encapsulation of curcumin loaded chitosan nanoparticle within poly (ϵ -caprolactone) and gelatin fiber mat for wound healing and layered dermal reconstitution. *Int J Biol Macromol.* 2020;153:1241–1250. doi: [10.1016/j.ijbiomac.2019.10.255](https://doi.org/10.1016/j.ijbiomac.2019.10.255).
- [53] Silva JC, Udangawa RN, Chen J, et al. Kartogenin-loaded coaxial PGS/PCL aligned nanofibers for cartilage tissue engineering. *Mater Sci Eng C Mater Biol Appl.* 2020;107:110291. doi: [10.1016/j.msec.2019.110291](https://doi.org/10.1016/j.msec.2019.110291).
- [54] Jeffries EM, Allen RA, Gao J, et al. Highly elastic and suturable electrospun poly (glycerol sebacate) fibrous scaffolds. *Acta Biomater.* 2015;18:30–39. doi: [10.1016/j.actbio.2015.02.005](https://doi.org/10.1016/j.actbio.2015.02.005).
- [55] Kim HH, Kim MJ, Ryu SJ, et al. Effect of fiber diameter on surface morphology, mechanical property, and cell behavior of electrospun poly (ϵ -caprolactone) mat. *Fibers Polym.* 2016;17(7):1033–1042. doi: [10.1007/s12221-016-6350-x](https://doi.org/10.1007/s12221-016-6350-x).
- [56] Kong Y, Tang X, Zhao Y, et al. Degradable tough chitosan dressing for skin wound recovery. *Nanotechnol Rev.* 2020;9(1):1576–1585. doi: [10.1515/ntrev-2020-0105](https://doi.org/10.1515/ntrev-2020-0105).
- [57] Movahedi M, Asefnejad A, Rafienia M, et al. Potential of novel electrospun core-shell structured polyurethane/starch (hyaluronic acid) nanofibers for skin tissue engineering: in vitro and in vivo evaluation. *Int J Biol Macromol.* 2020;146:627–637. doi: [10.1016/j.ijbiomac.2019.11.233](https://doi.org/10.1016/j.ijbiomac.2019.11.233).
- [58] Vogt L, Rivera LR, Liverani L, et al. Poly (ϵ -caprolactone)/poly (glycerol sebacate) electrospun scaffolds for cardiac tissue engineering using benign solvents. *Mater Sci Eng C Mater Biol Appl.* 2019;103:109712. doi: [10.1016/j.msec.2019.04.091](https://doi.org/10.1016/j.msec.2019.04.091).
- [59] Cheng G, Ma X, Li J, et al. Incorporating platelet-rich plasma into coaxial electrospun nanofibers for bone tissue engineering. *Int J Pharm.* 2018;547(1–2):656–666. doi: [10.1016/j.ijpharm.2018.06.020](https://doi.org/10.1016/j.ijpharm.2018.06.020).